School of Natural Sciences and Mathematics

2013-10-18

Electrochemically Gated Organic Photovoltaic with Tunable Carbon Nanotube Cathodes

UTD AUTHOR(S): Alexander B. Cook, Jonathan D. Yuen and Anvar A. Zakhidov

Alexander B. Cook, Jonathan D. Yuen, and Anvar Zakhidov

Articles you may be interested in

Effect of nano-filler on the performance of multiwalled carbon nanotubes based electrochemical double layer capacitors
J. Renewable Sustainable Energy **6**, 013108 (2014); 10.1063/1.4861889

Single carbon nanotube photovoltaic device
J. Appl. Phys. **114**, 164320 (2013); 10.1063/1.4828485

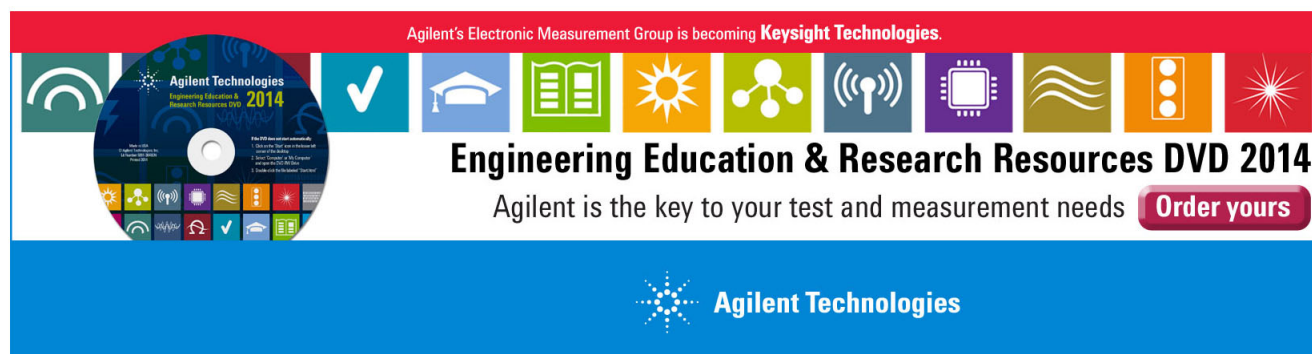Limits to the magnitude of capacitance in carbon nanotube array electrode based electrochemical capacitors
Appl. Phys. Lett. **102**, 173113 (2013); 10.1063/1.4803925

Multiwalled carbon nanotube sheets as transparent electrodes in high brightness organic light-emitting diodes
Appl. Phys. Lett. **93**, 183506 (2008); 10.1063/1.3006436

Gate capacitance in electrochemical transistor of single-walled carbon nanotube
Appl. Phys. Lett. **88**, 073104 (2006); 10.1063/1.2173626

Electrochemically gated organic photovoltaic with tunable carbon nanotube cathodes

Alexander B. Cook, Jonathan D. Yuen, and Anvar Zakhidov[a]

Physics Department and Alan G. MacDiarmid Nanotech Institute, University of Texas at Dallas, Richardson, Texas 75080, USA

We demonstrate an organic photovoltaic (OPV) device with an electrochemically gated carbon nanotube (CNT) charge collector. Bias voltages applied to the gate electrode reconfigure the common CNT electrode from an anode into a cathode which effectively collects photogenerated electrons, dramatically increasing all solar cell parameters to achieve a power conversion efficiency of ~3%. This device requires very little current to initially charge and the leakage current is negligible compared to the photocurrent. This device can also be viewed as a hybrid tandem OPV-supercapacitor with a common CNT electrode. Other regimes of operation are briefly discussed. © 2013 AIP Publishing LLC. [http://dx.doi.org/10.1063/1.4826145]

Polymer semiconductors are the leading organic photovoltaic (OPV) materials due to their high absorptivity, good transport properties, flexibility, and compatibility with temperature sensitive substrates. OPV efficiencies have jumped significantly in the past years, with single cell efficiencies as high as 9.1%,[1] making them an increasingly viable energy technology. These advances are due to improvements in the polymeric active layer; few of these advancements represent breakthroughs which truly challenge indium tin oxide (ITO) and aluminum, despite the high cost and processing limitations of those traditional electrodes. Cathode materials also limit OPV performance, with calcium and lithium fluoride, in conjunction with aluminum, commonly used. However, their low stability in air poses a problem, as does the lack of optical transparency and the requirement of high-vacuum processing. Zinc oxide and titanium oxide materials can be used to invert larger work function materials such as ITO,[2–4] but additional processing steps are required, and the high temperature of ITO processing prevents its application to multi-junction interlayers or inverted structures. This generates demand for transparent low work function materials for cathodes in OPV tandems and other optoelectronic devices.

Carbon nanotubes (CNT) have been demonstrated to function in OPV's as transparent anodes with 3-D bulk type collection of charges[5] and as interlayer electrodes in parallel tandem cells.[6] Transparent CNT sheets on top of n-doped C60 have been demonstrated as a cathode in a small molecule device.[7] The present work is further motivated by the discovery that the conductivity and work function of carbon nanotubes can be strongly modified by electric double layer charging (EDLC) in an electrolyte.[8–10] The work function shifts as much as $\pm 0.7\,\text{eV}$ in an aqueous electrolyte and is stable; the effect persists when the charged CNT are physically removed from the electrolyte.[8–11] The conductivity of EDLC CNT is enhanced by as much as an order of magnitude in mixed Single-Walled (SWCNT) and can shift by a factor of two in Multiwalled (MWCNT). These advantages motivated us to invent a hybrid tandem architecture in which the work function of the CNT electrode in an OPV is modified *in situ* by redistribution of ions from a supercapacitive ionic gate.

The hybrid tandem device described here is a monolithic, parallel combination of an OPV and a supercapacitor connected by a layer of highly porous CNT serving as the common electrode, as shown in Figure 1(a).[12] This design is somewhat similar to an n-Si/SWCNT Schottky solar cell designed by Wadhwa *et al.*,[13] but features a organic active layer and a significantly different physical behavior under gate bias. In our design, the parallel electrical configuration[14] allows a gate voltage bias (V_{GATE}) to be applied between the common and gate electrodes of the supercapacitor sub-cell, independent from the OPV cell (which generates power between the ITO and common electrodes). We chose an ionic liquid for the supercapacitor electrolyte as it is non-volatile, has a large potential window, does not dissolve the organic layers, and wets the CNT. This has been demonstrated in ionic liquid gated transistors.[15–17]

The photocurrent travels exclusively between the ITO anode and CNT common electrode of the OPV. This is distinct from dye sensitized solar cells (DSSC) in which photocurrent is carried by ionic conduction through the electrolyte via reduction reactions of dye at the photoelectrode and oxidation at the counter electrode.[18] Ionic liquids have also been utilized in a monolithic OPV structure in which EDLC charging enables AC transport of photocurrent via the electrolyte itself in recent work by Li *et al.*[19,20] In contrast, the electrolyte in our device functions to modify the work function of the CNT, and to partially dope adjacent organic polymer chains, not to transfer photocurrent.

Poly(3,4-ethylenedioxythiophene):poly-(styrenesulfonate) PEDOT:PSS from Heraeus (Clevios™ PVP AI 4083) was filtered through a 0.45 micron nylon filter and spin-coated onto UV-ozone treated, patterned ITO-glass substrates, resulting in a 30 nm thick layer. The substrates were annealed at 180 °C for 5 min. A 1:1 solution of poly(3-hexylthiophene-2,5-diyl) (P3HT: P200, Rieke Metals Inc.) and phenyl-C61-butyric acid methyl ester (PCBM: Nano-C) in chlorobenzene was then spun onto the PEDOT:PSS substrate, allowed to rest overnight, and then annealed at 170 °C

[a]Author to whom correspondence should be addressed. Electronic mail: zakhidov@utdallas.edu. Tel. 972-883-6218.
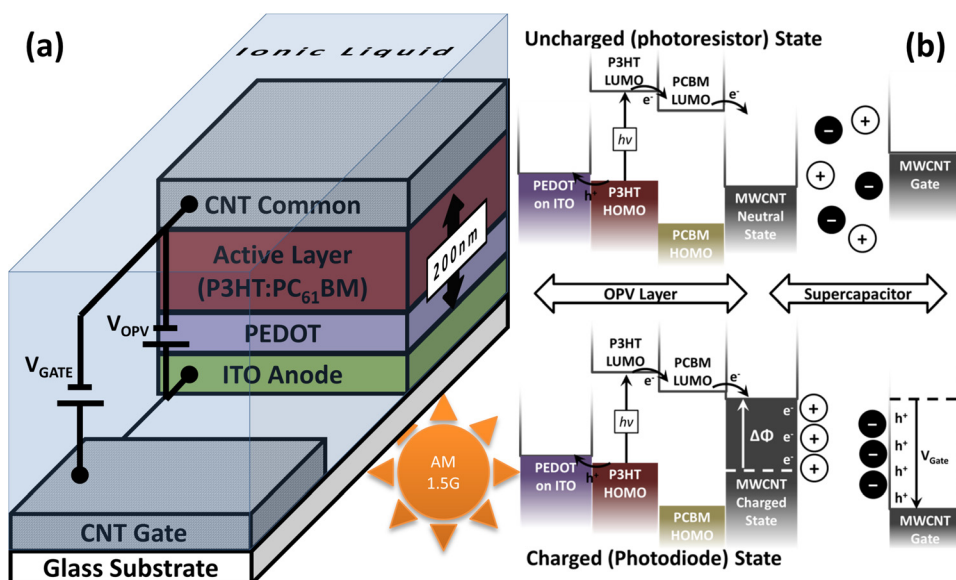
FIG. 1. (a) The structure of the hybrid monolithic OPV-Supercap Device. (b) The energy level diagram of the device in the uncharged (upper) and positive gated, i.e., EDLC charged (lower) state. Notice the decrease of work function, $\Delta\phi$, due to upward shift of Fermi level in CNT.

for 5 min. The total device thickness was measured to be 200 nm thick by a stylus profilometer.

Highly oriented CNT sheets approximately 3 mm wide were dry-pulled from a CNT forest synthesized at UTD, and laid on top of the P3HT:PCBM layer.[21,22] After five layers were laid, the carbon nanotubes were densified with 3M™ Novec™ 7100 Engineered Fluid, methoxy-nonafluorobutane ($C_4F_9OCH_3$). An additional five layers were applied to the bare glass and ITO on the far side of the device to serve as a gate electrode. Contacts were created using silver paint. A drop (10 μl) of ionic liquid, N,N-Diethyl-N-methyl-N-(2-methoxyethyl) ammonium tetrafluoroborate, DEME-BF$_4$ (Kanto Chemical Co. Inc.), was placed on top of both CNT electrodes. A glass microscope cover-slip was placed on the ionic liquid to spread and contain it. As the ionic liquid is non-volatile and viscous, sealing is not needed. The ionic liquid thickness is estimated to be around 50–100 μm.

OPV measurements were carried out in a nitrogen glove box with an AM 1.5G calibrated solar simulator and two Keithley 2400 source measure units (SMU) controlled by a

LabVIEW™ program. Using two SMUs allowed a gate voltage (V_{GATE}) to be applied to the supercapacitor while the second SMU measures the resulting solar cell parameters. A 1 mm diameter precision-pinhole aperture from Edmund Optics was employed to mask the device during testing.

In this Letter, we will summarize the results of two different measurements: Current-voltage (IV) sweeps of the OPV with constant V_{GATE} across the supercapacitor. Second, open-circuit voltage (V_{OC}) and short-circuit current density (J_{SC}) measured as a function of V_{GATE}. This secondary measurement gives a picture of the device characteristics in its steady state condition, as compared to the relatively fast IV sweeps.

The reconfigurability of the hybrid device is most dramatically found in the OPV IV characteristics. Voltage sweeps from −0.8 V to 0.8 V and back were performed under AM 1.5G illumination and in the dark. Prior to the inclusion of ionic liquid, the IV characteristics are purely ohmic; i.e., show a linear relation between current and voltage. We reconfigured this symmetric device (which is not an OPV
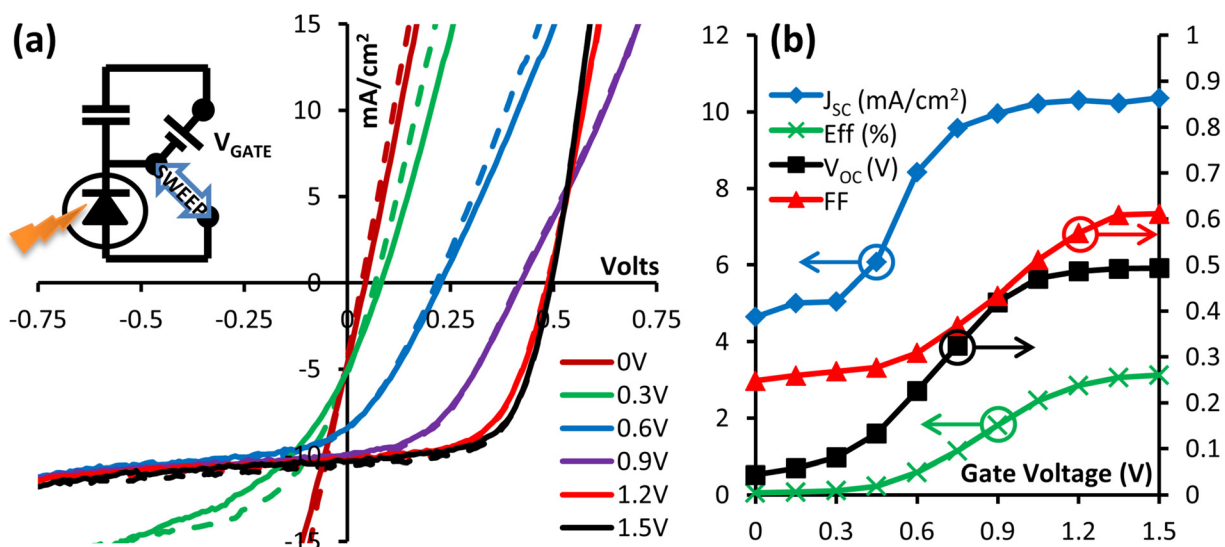

FIG. 2. (a) The IV curves under illumination. The solid lines indicate sweeps from low voltages to high, and the dashed lines indicate sweeps in the reverse direction. The inset shows an approximate circuit diagram. (b) The extracted parameters for the OPV subcell as a function of V_{GATE}.

yet) by charging the capacitor, waiting 5 min for stabilization, and then running a set of five sweeps. The findings from the final voltage sweep in each set are shown in Figure 2(a). The results clearly show a good OPV performance, progressing from a "hole-only" photoresistor into a photodiode.

We observed little change in the IV characteristics before inclusion of ionic liquid and afterwards with a gate voltage of 0 V as shown in the supplementary material.[23] However, with $V_{GATE} = 0.3$ V, we start to see photodiode-like IV characteristics overlaid on the ohmic characteristics. The photodiode behavior becomes stronger and the ohmic character weakens as V_{GATE} increases with a threshold around $V_{GATE} = 0.4$-0.5 V. At $V_{GATE} = 1.5$ V, the IV characteristics are those of a good photodiode. With moderate gate voltages, we observe some hysteresis in the IV curves; probably from additional charging/discharging of the CNT common electrode from the OPV IV sweep.

The changes of V_{OC}, J_{SC}, fill-factor (FF), and external efficiency (Eff), derived from Figure 2(a), are plotted as a function of V_{GATE} in Figure 2(b). Below $V_{GATE} = 0.3$-0.4 V, the parameters do not increase significantly. Above $V_{GATE} = 0.5$ V, a sharp rise in all four parameters (V_{OC}, I_{SC}, FF, and Eff) occurs. With the exception of FF and Eff, the increases taper off after $V_{GATE} = 0.9$ V–1 V. We note that the maximum parameters achieved almost match the best regular structured P3HT:PC$_{61}$BM cell, and that the series resistance in the forward bias of the highly charged state surpasses the series resistance prior to charging.

A complementary experiment confirmed the findings described above. In this case, V_{OC} or J_{SC} was dynamically measured as V_{GATE} was incrementally increased from 0 to 1.5 V and back in 0.1 V increments per 5 min. We note that these results are from a different device which is constructed in a similar manner, which results in slightly different threshold and saturation gate voltage values. These variations are a consequence of slightly differing active areas and relative electrode sizes. We generally observe that V_{OC} and J_{SC} saturate 2–3 min after a voltage step. In Figure (3), V_{OC} and J_{SC} values obtained at the end of each 5 min interval is shown. The detailed dynamics of the charging will be discussed elsewhere, while here we describe the general tendencies found.
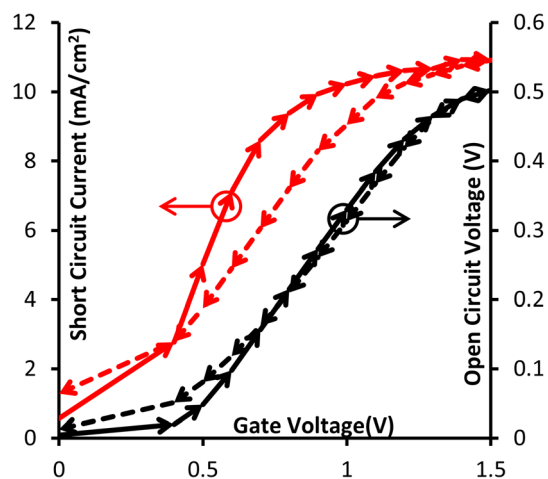

FIG. 3. The charging and discharging curves for the Voc and Jsc of the OPV. Each bias voltage step was held for 5 min. The dotted line is the discharging (1.5-0V$_{GATE}$) sweep.

Initially, we observe that J_{SC} and V_{OC} were close to zero as in our previous results. Similarly, we observe a rapid increase in J_{SC} and V_{OC} occurs around threshold $V_{GATE} = 0.4$ V, as V_{GATE} is increased. Again, J_{SC} saturates at a lower V_{GATE} does than V_{OC}, with the onset of saturation for J_{SC} at $V_{GATE} = 0.9$ V and $V_{GATE} = 1.4$ V for V_{OC}. When V_{GATE} is decreased, we observe no significant variations in the dependence of V_{OC} on V_{GATE}. However, a hysteresis effect is observed in J_{SC}.

Additionally, we measured the discharging rate of these devices. In this experiment, the supercapacitor was charged at $V_{GATE} = 1.5$ V for 5 min, then disconnected from the power supply leaving an open circuit between the CNT gate and CNT common electrodes. As the device discharged, the variation in V_{OC} and J_{SC} over time was monitored. We observed that V_{OC} and J_{SC} decreased slowly in a somewhat exponential fashion over the course of half an hour. V_{OC} discharged more rapidly than J_{SC}, requiring 22 min to reach half its initial value, while J_{SC} required 33 min. This follows the observations made concerning the dependence of V_{OC} and J_{SC} on V_{GATE}. Since J_{SC} saturates at a smaller V_{GATE} than V_{OC}, we expect J_{SC} to decrease less rapidly than V_{OC} as V_{GATE} discharges. The plots of this data are depicted in the supplementary material.[23]

To understand the preceding results, consider Figures 1(b) and 1(c) which shows the energy levels as EDLC of opposite polarities are formed on the CNT-ionic liquid interface of each electrode. In-situ EDLC charging injects a large electronic charge into CNTs, due to the giant capacitance of CNT arising from the huge interface area. Kuznetsov estimated the charge stored in the CNT electrodes to be on the order of 5.8×10^{20} ions per cm^3 or roughly one ion per fifty carbon atoms in the case of aqueous electrolytes in his thesis.[11] The injected charge significantly shifts the Fermi level of CNT and hence effective work function as the CNT fill with either electrons or holes. Without charging, the ITO/PEDOT:PSS and CNT electrodes are nearly symmetric in work function, but PEDOT:PSS may block electrons giving some small photocurrent at zero V_{GATE}. As such, there is no internal field for separation and collection of photo-generated charges. A positive gate voltage (V_{GATE}) at between the CNT common electrode and the gate electrode decreases the common CNT electrode work function by electron injection, i.e., n-type doping of CNT. The common electrode begins collecting electrons rather than holes, and a photodiode forms, as shown in Figure 1(c).

The modulation of series and shunt resistances of the device reveals a little more information about the origin of the transition from ohmic photoresistor into photodiode as the V_{GATE} is increased. We note that in the range of $V_{GATE} = 0$ V-0.6 V the shunt resistance (R_{SH}) rapidly increases and then saturates. This can be clearly observed from the inverse of the slope of the IV curves in the reverse bias. The series resistance (R_S) increases at a moderate rate up to $V_{GATE} = 0.9$ V, but decreases rapidly for $V_{GATE} > 0.9$ V.

R_{SH} is the resistance between the ITO anode and CNT common electrode of the OPV. Initially, this resistance is low due to the ohmic contact between PEDOT:PSS, P3HT and the uncharged MWCNT. However, as the CNT are

charged and their work function increases, a barrier to hole transport is created and correspondingly the R_{SH} increases. In another words R_{SH} describes the charge selectivity of the electrodes: for a good cathode, the photogenerated holes are not collected at the cathode, which is indeed observed as R_{SH} increases.

Finally we address the question: does the energy required to charge the device detract from the power generated in the photovoltaic? We estimate that the energy stored in the CNT gate and CNT common electrodes during the initial charging is on the order of $2 J/m^2$, which is generated during approximately 70 ms of OPV device operation. See supplementary material for calculations.[23] Furthermore, the power required to maintain the charge appears to be on the order of $1.6 mW/m^2$. This is approximately six orders of magnitude smaller than the incident solar power, so is negligible in comparison.

This architecture may also provide insight into nonlinear physical processes in a coupled ionic-electronic system, as the hysteresis might be examined in terms of memristive behavior as recently discussed in inorganic oxides.[24] The *in-situ* doping of CNT by EDLC tunes not only work function but also the conductivity of the CNT and creates surface dipolar properties. This wide tuning of properties of CNT in-situ in a monolithic device can be applied to other types of hybrid functional devices, particularly photochargeable OPV in which the positive charging of CNT anode in the inverted OPV, leads to storage of energy in p-doped CNT electrode.[12] Similarly CNT with ionic liquid in its pores allows design of organic transistors and organic light emitting diodes with reconfigurable electrode.[25]

We have demonstrated an OPV-supercapacitor hybrid tandem of unique functionality. Charging the supercapacitor shifts the work function of the common CNT electrode by up to 0.7 eV turning it into a good cathode. This shift is attributed to injection of electrons into CNT by EDLC. This charge injection is very large due to the large surface area to mass ratio of the CNT, and the large effect on the work function can be attributed to the relatively small density of states with 1D singularities. Solar cell parameters increase from nearly zero up to values comparable with the best P3HT:$PC_{61}BM$ devices. Estimates based on our experimental results on charging and discharging currents show that the energy for charging CNT and maintaining the n-doped state of CNT is much smaller than energy photogenerated by the OPV.

[1]Z. He, C. Zhong, S. Su, M. Xu, H. Wu, and Y. Cao, Nature Photon. **6**, 591 (2012).

[2]G. Li, C.-W. Chu, V. Shrotriya, J. Huang, and Y. Yang, Appl. Phys. Lett. **88**, 253503 (2006).

[3]W. J. E. Beek, M. M. Wienk, M. Kemerink, X. Yang, and R. A. J. Janssen, J. Phys. Chem. B **109**, 9505 (2005).

[4]J. Y. Kim, S. H. Kim, H.-H. Lee, K. Lee, W. Ma, X. Gong, and A. J. Heeger, Adv. Mater. **18**, 572 (2006).

[5]R. Ulbricht, S. B. Lee, X. Jiang, K. Inoue, M. Zhang, S. Fang, R. H. Baughman, and A. Zakhidov, Sol. Energy Mater. Sol. Cells **91**, 416 (2007).

[6]S. Tanaka, K. Mielczarek, R. Ovalle-Robles, B. Wang, D. Hsu, and A. A. Zakhidov, Appl. Phys. Lett. **94**, 113506 (2009).

[7]Y. H. Kim, L. Müller-Meskamp, A. A. Zakhidov, C. Sachse, J. Meiss, J. Bikova, A. Cook, A. Zakhidov, and K. Leo, Sol. Energy Mater. Sol. Cells **96**, 244 (2012).

[8]A. A. Zakhidov, D.-S. Suh, A. A. Kuznetsov, J. N. Barisci, E. Muñoz, A. B. Dalton, S. Collins, V. H. Ebron, M. Zhang, J. P. Ferraris, A. Zakhidov, and R. H. Baughman, Adv. Funct. Mater. **19**, 2266 (2009).

[9]A. A. Kuznetzov, S. B. Lee, M. Zhang, R. H. Baughman, and A. Zakhidov, Carbon **48**, 41 (2010).

[10]D.-S. Suh, R. H. Baughman, and A. Zakhidov, U.S. patent application 8,101,061 (March 4, 2005).

[11]A. A. Kuznetzov, "Physics of electron field emission by self-assembled carbon nanotube arrays," Ph.D. thesis (The University of Texas at Dallas, 2008).

[12]A. Cook, J. D. Yuen, and A. Zakhidov, U.S. patent application 61,732,379 (December 2, 2012).

[13]P. Wadhwa, B. Liu, M. A. McCarthy, Z. Wu, and A. G. Rinzler, Nano Lett. **10**, 5001 (2010).

[14]A. Zakhidov, K. Mielczarek, and A. Papadimitratos, WIPO patent 2012106002. (July 6, 2012).

[15]Y. Xia, J. H. Cho, J. Lee, P. P. Ruden, and C. D. Frisbie, Adv. Mater. **21**, 2174–2179 (2009).

[16]H. Okimoto, T. Takenobu, K. Yanagi, Y. Miyata, H. Shimotani, H. Kataura, and Y. Iwasa, Adv. Mater. **22**, 3981–3986 (2010).

[17]T. Fujimoto, M. M. Matsushita, and K. Awaga, J. Phys. Chem. C **116**, 5240–5245 (2012).

[18]M. Grätzel, Nature **414**, 338 (2001).

[19]B. Li, Y. Noda, L. Hu, H. Yoshikawa, M. M. Matsushita, and K. Awaga, Appl. Phys. Lett. **100**, 163304 (2012).

[20]B. Li, S. Dalgleish, Y. Miyoshi, H. Yoshikawa, M. M. Matsushita, and K. Awaga, Appl. Phys. Lett. **101**, 173302 (2012).

[21]J. A. Velten, J. Carretero-González, E. Castillo-Martínez, J. Bykova, A. Cook, R. Baughman, and A. Zakhidov, J. Phys. Chem. C **115**, 25125 (2011).

[22]M. Zhang, S. Fang, A. Zakhidov, S. B. Lee, A. E. Aliev, C. D. Williams, K. R. Atkinson, and R. H. Baughman, Science **309**, 1215 (2005).

[23]See supplementary material at http://dx.doi.org/10.1063/1.4826145 for charging curves, calculations, and discharging curves.

[24]D. B. Strukov, G. S. Snider, D. R. Stewart, and R. S. Williams, Nature **453**, 80 (2008).

[25]J. D. Slinker, J. A. DeFranco, M. J. Jaquith, W. R. Silveira, Y.-W. Zhong, J. M. Moran-Mirabal, H. G. Craighead, H. D. Abruña, J. A. Marohn, and G. G. Malliaras, Nature Mater. **6**, 894 (2007).